

Volcanic Climate Warming through Radiative and Dynamical Feedbacks of SO₂ Emissions

Scott D. Guzewich¹, Luke D. Oman¹, Jacob Richardson², Patrick Liam Whelley³, Sandra T Bastelberger⁴, Kelsey Young¹, Jacob E Bleacher¹, Thomas Fauchez⁵, and Ravi Kopparapu⁶

¹NASA Goddard Space Flight Center

²NASA GSFC

³Goddard Space Flight Center (NASA)

⁴University of Maryland College Park

⁵Universities Space Research Association

⁶Unknown

November 21, 2022

Abstract

Volcanic flood basalt eruptions have been linked to or are contemporaneous with major climate disruptions, ocean anoxic events, and mass extinctions throughout at least the last 400M years of Earth's history. Previous studies and recent history have shown that volcanically-driven climate cooling can occur through reflection of sunlight by H₂SO₄ aerosols, while longer-term climate warming can occur via CO₂ emissions. We use the Goddard Earth Observing System Chemistry-Climate Model to simulate a four-year duration volcanic SO₂ emission of the scale of the Wapshilla Ridge member of the Columbia River Basalt eruption. Brief cooling from H₂SO₄ aerosols is outweighed by dynamically and radiatively driven warming of the climate through a three orders of magnitude increase in stratospheric H₂O vapor.

Volcanic Climate Warming through Radiative and Dynamical Feedbacks of SO₂ Emissions

Scott D. Guzewich^{1,6*}, Luke D. Oman^{1,6}, Jacob A. Richardson^{2,1,5,6}, Patrick L. Whelley^{2,1,5,6}, Sandra T. Bastelberger^{2,1,5,6}, Kelsey E. Young¹, Jacob E. Bleacher^{3,1}, Thomas J. Fauchez^{4,1,6}, Ravi K. Kopparapu^{1,6}

¹NASA Goddard Space Flight Center; Greenbelt, MD, USA.

²University of Maryland, College Park, MD, USA.

³NASA Headquarters, Washington, DC, USA.

⁴Universities Space Research Association, Columbia, MD, USA.

⁵Center for Research and Exploration in Space Science and Technology, NASA/GSFC, Greenbelt, MD, USA 20771

⁶NASA GSFC Sellers Exoplanet Environments Collaboration, Greenbelt, MD, USA 20771

1 Corresponding author: Scott D. Guzewich (scott.d.guzewich@nasa.gov)

2 **Key Points:**

- 3 • Volcanic emission of SO₂ produces warming through climate feedbacks.
- 4 • The warming is driven by a three orders of magnitude increase in stratospheric H₂O
- 5 vapor.
- 6 • Climate cooling by H₂SO₄ aerosols persists for less time than the eruption itself.
- 7

8 **Abstract**

9 Volcanic flood basalt eruptions have been linked to or are contemporaneous with major climate
10 disruptions, ocean anoxic events, and mass extinctions throughout at least the last 400M years of
11 Earth's history. Previous studies and recent history have shown that volcanically-driven climate
12 cooling can occur through reflection of sunlight by H₂SO₄ aerosols, while longer-term climate
13 warming can occur via CO₂ emissions. We use the Goddard Earth Observing System Chemistry-
14 Climate Model to simulate a four-year duration volcanic SO₂ emission of the scale of the Wapshilla
15 Ridge member of the Columbia River Basalt eruption. Brief cooling from H₂SO₄ aerosols is
16 outweighed by dynamically and radiatively driven warming of the climate through a three orders
17 of magnitude increase in stratospheric H₂O vapor.

18 **Plain Language Summary**

19 Volcanic flood basalt eruptions are linked to mass extinctions and climate change through Earth's
20 history. Using model experiments, we show that a massive release of sulfur dioxide gas, as would
21 happen in such an eruption, can warm the climate through feedback mechanisms linked to an
22 increase in stratospheric water vapor.

23 **1 Introduction**

24 Flood basalt eruptions are the largest in Earth's history by volume of emitted material (Rampino
25 et al., 1998; Self et al., 2005; Reichow et al., 2009). They have covered vast areas with basalt,
26 released massive amounts of climatically-relevant gases into the atmosphere, and are nearly
27 contemporaneous with many of Earth's mass extinctions or ocean anoxic events (Wignall, 2001;
28 Courtillot and Renne, 2003; Sobolev et al., 2011). Flood basalts appear common on other
29 terrestrial worlds in the Solar System (Bond and Sun, 2021; Head et al., 2011; Lancaster et al.,
30 1995; Jaeger et al., 2010; O'Hara, 2000). Unlike explosive eruptions of stratovolcanoes such as
31 Toba, Tambora, and Pinatubo that last only for hours to weeks, flood basalt eruptions continue for
32 years if not millenia (Courtillot and Renne, 2003; Jerram and Widdowson, 2005; Barry et al.,
33 2010). The climate impact of such eruptions is still being debated in the literature with the cooling
34 provided by shortwave sunlight reflection from H₂SO₄ aerosols balanced against the warming
35 influence of CO₂ emissions (Self et al., 2005; Schmidt et al., 2016; Self et al., 2006; Black et al.,
36 2018; Armstrong McKay et al., 2014). Such eruptions have been implicated in producing
37 "hyperthermal" periods in Earth's history such as the Permian-Triassic hothouse and the
38 Paleocene-Eocene Thermal Maximum, but the volume of emitted CO₂ seems insufficient for such
39 warming (Bond and Sun, 2021; Gutjahr et al., 2017).

40 The Columbia River Basalt (CRB) eruption occurred 15-17 Ma in the Pacific Northwest of the
41 United States (Kasbohm and Schoene, 2018; Reidel, 2015). It is the smallest continental flood
42 basalt eruption and the most historically recent. It occurred near the Mid-Miocene Climatic
43 Optimum (MMCO), a globally warm period with possibly enhanced atmospheric CO₂ levels, and
44 just before the Mid-Miocene Climate Transition (MMCT), a period of cooling climate and
45 increasing polar glaciation associated with a significant extinction event (Foster et al., 2012). The
46 CRB has been proffered as a mechanism to drive either climate warming (as during the MMCO)
47 or cooling (as during the MMCT) (Schmidt et al., 2016; Hodell and Wodruuff, 1994; Kürschner et
48 al., 2008; Sosdian et al., 2020). The Wapshilla Ridge member of the Grande Ronde basalt, one
49 member of the CRB group, was responsible for 20% of the CRB's emitted volume and may have
50 emitted up to 300 Gt of SO₂ into the atmosphere (Kasbohm and Schoene, 2018; Davis et al., 2017

51). For reference, this amount is ~20,000 times the SO₂ emitted by the eruption of Mt. Pinatubo in
52 1991 (Bluth et al., 1992). CRB eruptions were likely a mix of explosive events that sent material
53 high into the upper troposphere and lower stratosphere (~13-17 km altitude) and effusive eruptions
54 that did not extend above 3 km altitude (Glaze et al., 2017).

55 Our study examines the climate response to the long duration and massive SO₂ release by such an
56 eruption in the Goddard Earth Observing System Chemistry-Climate Model (GEOSCCM). A
57 model such as GEOSCCM is needed to self-consistently model the conversion of SO₂ to H₂SO₄
58 aerosols, the radiative response to those aerosols, and the dynamical response to the eruption.
59 Using the Wapshilla Ridge member of the CRB eruption as a template and scaling by 1/10, we
60 emit 30 Gt of SO₂ into the model over four years through a 80%/20% mix of explosive and effusive
61 eruptions, respectively (Davis et al., 2017, **Fig. S1**). We use a pre-industrial atmosphere with a
62 fixed concentration of 280 ppm of CO₂, levels of ozone-depleting substances appropriate for the
63 year 1850, and otherwise modern surface boundary and initial conditions to isolate the climate
64 response to the SO₂ release through an eruption simulation and a baseline simulation without it.
65 SO₂ is not radiatively active in the model.

66 **2 Materials and Methods**

67 We conduct two Goddard Earth Observing System Chemistry Climate Model (GEOSCCM)
68 simulations for this work. The first is a baseline simulation without addition of volcanically-
69 sourced SO₂. The second is the volcanic eruption scenario that releases SO₂ at model gridpoints
70 in eastern Washington state and Oregon (corresponding to the CRB vents) following the volcanic
71 eruption scenario detailed below. Both simulations run for 20 years. The simulations use
72 modern initial and boundary conditions with a pre-industrial atmosphere. The atmosphere has a
73 fixed CO₂ concentration of 280 ppm and ozone-depleting substances at levels appropriate for the
74 year 1850. SO₂ is radiatively inert in the model.

75

76 2.1. Goddard Earth Observing System Chemistry Climate Model (GEOSCCM)

77

78 We use the GEOSCCM, which couples a general circulation model (Rienecker et al., 2008; Nielsen
79 et al., 2017) with dynamic ocean and sea ice modules (Aquila et al., 2021) and a comprehensive
80 Global Modeling Initiative (GMI) stratosphere-troposphere chemical mechanism (Duncan et al.,
81 2007; Strahan et al., 2007), to assess the atmosphere-ocean-chemistry coupled response to a CRB-
82 type volcanic perturbation. The model is integrated with the Goddard Chemistry, Aerosol,
83 Radiation, and Transport (GOCART) bulk aerosol module (Colarco et al., 2010), to simulate
84 aerosol evolution and transport and its effect on radiation.

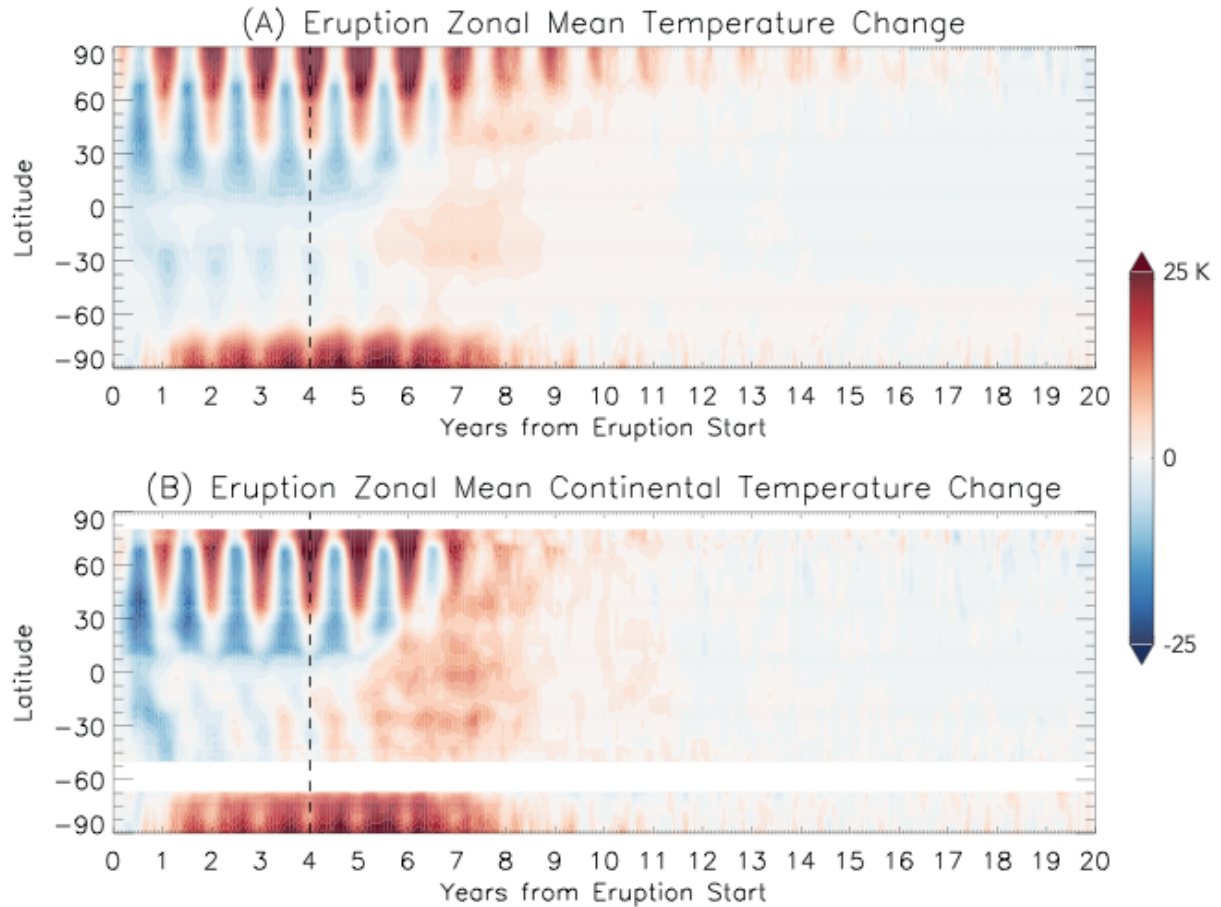
85 The GMI chemical mechanism includes 117 species, 322 chemical reactions, and 81 photolysis
86 reactions. The SMVGEAR II algorithm (Jacobson et al., 1995) is used to integrate the chemical
87 mass balance equations. The mechanism includes a detailed description of O₃-NO_x-hydrocarbon
88 chemistry, which is described in (Duncan et al., 2007). In order to better understand the feedbacks
89 to climate these simulations used a dynamic ocean, from the Modular Ocean Model, Version 5
90 (MOM5) (Griffies et al., 2005; Griffies et al., 2012), and the Los Alamos Sea Ice Model (CICE)
91 (Hunke et al., 2008). The simulations used a horizontal resolution of 1° longitude by 1° latitude in
92 the atmosphere and ocean components. The atmosphere has 72 vertical levels from the surface to
93 ~80 km and the ocean component has 50 layers down to a depth of 4,500 m.

94 **2.2. Columbia River Volcanic Eruption Scenario**

95 Our Columbia River Flood Basalt eruption scenario is informed by the eruption dynamics of the
96 Wapshilla Ridge Member of the Grande Ronde Basalt Group within the CRB. As the Wapshilla
97 Ridge Member represents the largest flow unit of the Grande Ronde, which in turn was the largest
98 phase of the CRB, this simulated eruption provides a high-end view of the short-term climate
99 effects produced by the CRB. Total erupted SO₂ of the Wapshilla Ridge was likely 300 Gt
100 (Kasbohm and Schoene, 2018; Davis et al., 2017) and thermal modeling informed by geothermal
101 alteration of host rocks near Wapshilla vents provides an eruption duration of as low as 4 years
102 (Davis et al., 2017). Assuming that the Wapshilla Ridge was formed through multiple eruptive
103 episodes (e.g., Davis et al., 2017), our scenario erupts one-tenth of the total estimated SO₂ mass,
104 30 Gt, over 4 calendar years. Around 20% of the SO₂ delivered to that atmosphere during this
105 eruptive phase passively outgassed from the lava flow itself, with the remaining 80% directly
106 vented from the fissure. Following (Glaze et al., 2017), we assume that the Wapshilla fissure vents
107 periodically erupted SO₂ into the Upper Troposphere-Lower Stratosphere (UTLS) from 13-18 km
108 altitude. We deliver the final 20% of the gas to the Planetary Boundary Layer (PBL) and lower
109 troposphere (<3 km altitude). To minimize seasonal effects, UTLS injections of SO₂ are divided
110 into 4 discrete “eruptions” per year, equally spaced over each calendar. PBL injections, however,
111 are constant.

112 **3 Results**

113 The initial response to the eruption is rapid cooling, particularly focused over northern hemisphere
114 continental areas (**Fig. 1**). Global mean temperatures cool by 2-3 K in the first two years following
115 the eruption. However, July and August monthly mean temperatures over northern hemisphere
116 continents are 10-30 K colder than a baseline simulation (**Fig. S2**). The coldest temperature
117 anomalies are in central and southwest Asia. Southern hemisphere continents experience more
118 modest cooling in the first two years, but still experience temperatures 5-15 K below a baseline
119 simulation, with the coldest area relative to normal in central South America south of the Amazon
120 basin. Most of Antarctica’s surface area warms 2-8 K, however. By the first northern hemisphere
121 winter following the beginning of the eruption, these cold temperature anomalies are reversed and
122 8-15 K warm anomalies blanket the Arctic, Siberia, and north-central North America. Some 5-15
123 K cold anomalies remain over Australia, South Africa, and Argentina, but they are small in area
124 relative to northern hemisphere summer. This winter warming and summer cooling is a well-
125 known response to other volcanic eruptions, including Pinatubo (Kirchner et al., 1999). The
126 summer cooling is a direct response to the reduction in incoming solar radiation by the volcanic
127 aerosols, while the winter warming is a dynamically indirect response to a strengthened winter
128 stratospheric polar vortex (Kirchner et al., 1999). This is true in our simulation as well with an
129 extremely cold stratospheric winter polar vortex throughout the eruption years and for several
130 years after. In fact, the stratospheric winter polar vortex sees temperatures as low as -158 to -
131 168°C, cold enough to condense CO₂ (although such physics are not included in GEOSCCM).



132

133 **Fig. 1. Zonal mean temperature change of the eruption simulation relative to a baseline.** (A)
 134 Zonal mean temperature change (K) of the eruption simulation relative to a 20-year average of a
 135 baseline simulation as a function of time and (B) the zonal mean temperature change over
 136 continental areas only. The vertical dashed line represents the end of the eruption.

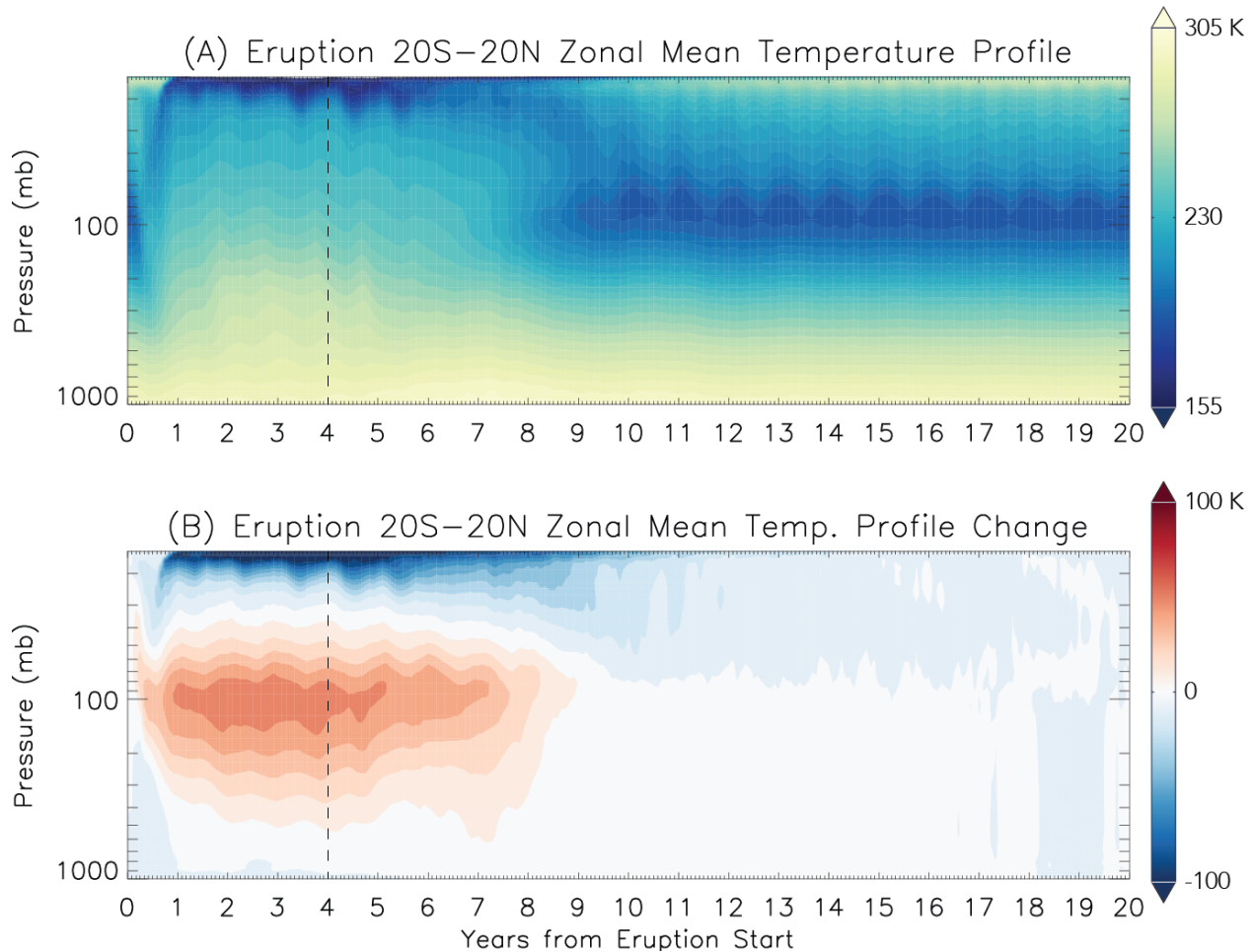
137

138 The cooling response to large volcanic eruptions is well-known in the literature and in modern
 139 history (Schmidt et al., 2016; Self et al., 2006; Black et al., 2018; Kirchner et al., 1999; Stoffel et
 140 al., 2015; Robock, 2000). SO_2 is rapidly and efficiently converted to H_2SO_4 aerosols, which are
 141 optically reflective and scatter incoming solar shortwave radiation back to space (Robock, 2000).
 142 Indeed, the volume of emitted SO_2 is so large that the global area-weighted H_2SO_4 550 nm aerosol
 143 optical thickness (AOT) exceeds 40 at the end of the first year following the start of the eruption.
 144 At the conclusion of the eruption in year four, global mean AOT reaches almost 220 (**Fig. S3**).
 145 The thickest aerosol layer remains concentrated in the northern hemisphere throughout the
 146 eruption and extends throughout the troposphere and stratosphere. Even the northern hemisphere
 147 surface atmosphere has part-per-million (ppm) level H_2SO_4 aerosol mixing ratios with the
 148 maximum aerosol concentrations occurring at 200 hPa.

149 This extremely opaque aerosol layer radically alters the planet's net radiative budget (**Fig. S4, S5**).
 150 It drives a 140-150 W/m^2 reduction in surface downward shortwave radiation flux and a somewhat
 151 larger (180 W/m^2) decrease in planetary outgoing longwave radiation. Concurrently, there is a

152 brief 35% reduction in global cloud cover (**Fig. S5**) with a nearly order-of-magnitude reduction in
153 precipitation rate (**Fig. S6**). Past research has also implied that large volcanic eruptions reduce
154 monsoon intensity in the northern hemisphere (Zambri et al., 2017). Our eruption simulation
155 similarly sees a drastic reduction of Indian and southeast Asian monsoon precipitation (and
156 throughout the northern hemisphere summer intertropical convergence zone) during the eruption
157 and for 4-6 years after, before a multiyear period with enhanced monsoon precipitation coinciding
158 with the warmest global temperature anomalies (**Fig. S7**). We also see dramatically increased
159 precipitation in South America, particularly the Pacific coast of Ecuador and Peru.

160 Despite the initial near-surface cooling, the very thick H₂SO₄ aerosol layer efficiently absorbs
161 longwave radiation from the surface (Kirchner et al., 1999) and warms the troposphere and
162 stratosphere. Tropical (20°S-20°N) temperature profiles warm through the troposphere and
163 become more stable. However, this warming also completely eliminates the tropical tropopause—
164 the atmosphere's cold trap for water vapor. Tropical tropopause temperatures warm by as much
165 as 60 K and this occurs rapidly following the initial months of the eruption, even while the surface
166 and lower troposphere are still cooling (**Fig. 2**). Indeed, during and continuing for almost four
167 years after the end of the eruption, there is no tropical temperature inversion in monthly mean
168 vertical temperature profiles. Despite a less convectively unstable vertical temperature profile, the
169 complete lack of a temperature inversion allows water vapor to flood into the stratosphere. Starting
170 almost immediately after the eruption begins, stratospheric water vapor levels increase by up to
171 three orders-of-magnitude (**Fig. 3**), reaching part-per-thousand mixing ratios, neatly following the
172 Clausius-Clapeyron relation for such a temperature change in the upper troposphere and
173 stratosphere.

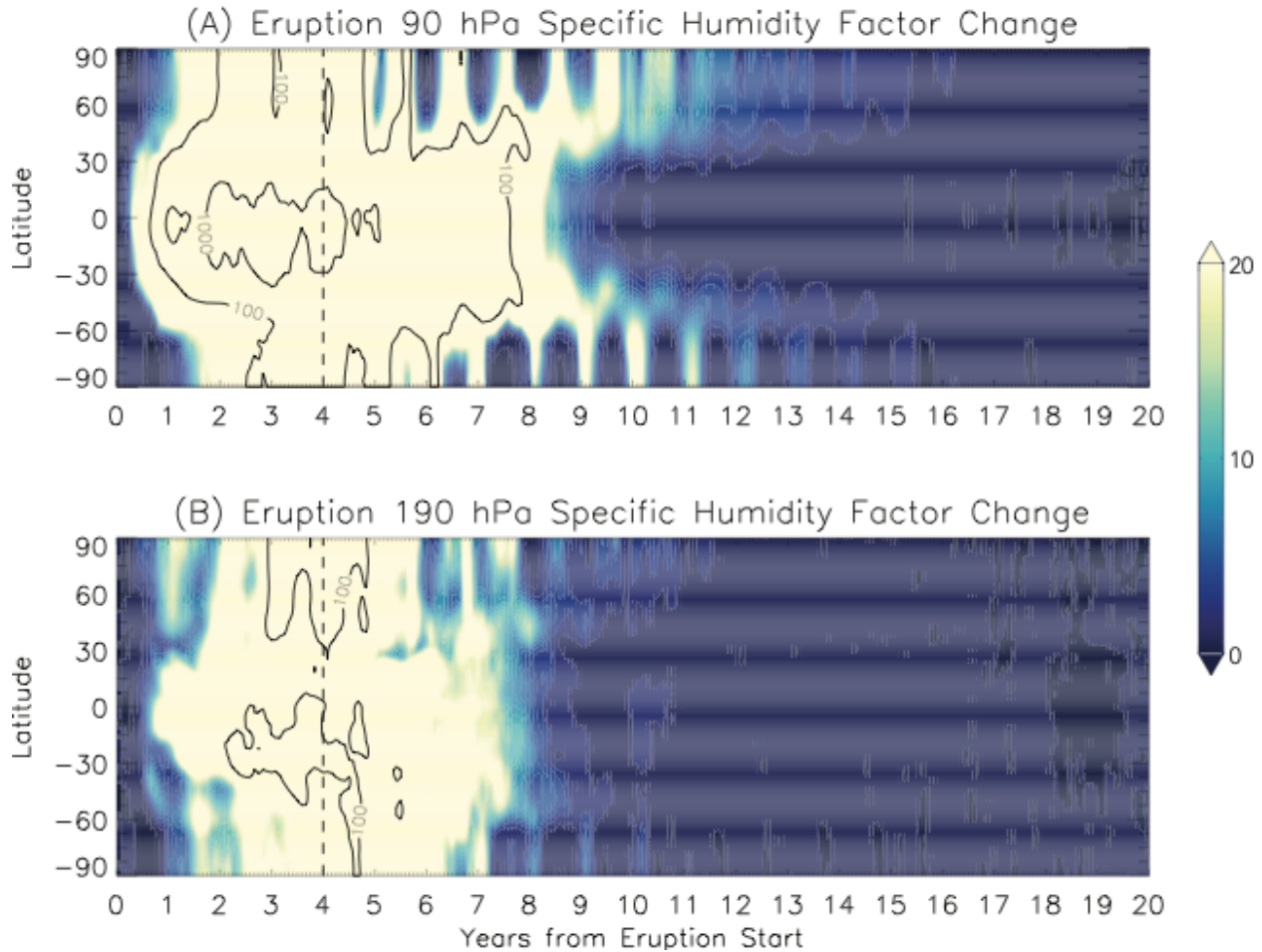


174

175 **Fig. 2. Vertical temperature profile response to the eruption.** (A) Zonal mean vertical
 176 temperature (K) profile in the tropics (20°S-20°N) of the eruption simulation as a function of time
 177 and pressure and (B) the change in the vertical temperature profile relative to a baseline simulation.
 178 The vertical dashed line represents the end of the eruption.

179

180 It is this change to stratospheric water vapor mixing ratios that is responsible for the subsequent
 181 climate warming. Rather than having a strengthening net cooling response due to the increasing
 182 aerosol optical thickness over the four years of the eruption, downward longwave flux from this
 183 stratospheric water vapor counteracts the reduction in surface shortwave flux. This water vapor
 184 provides 50 W/m^2 of downward longwave flux at the surface when the stratospheric water vapor
 185 mixing ratio is maximized. This causes global mean surface temperatures to return to those of the
 186 baseline simulation prior to the end of the eruption, late in the fourth year of the simulation. Global
 187 temperatures continue to warm well past the end of the eruption, peaking nearly four years later
 188 with global mean surface temperature anomalies of +5-6 K (**Fig. 1**). At this point, typical
 189 seasonality also returns to global mean temperatures with an annual minimum in northern
 190 hemisphere winter and maximum in northern summer.



191

192 **Fig. 3. Stratospheric water vapor increases as a result of the eruption.** (A) Factor change in
 193 the zonal mean specific humidity at the 90 hPa pressure level in the eruption simulation relative to
 194 the baseline simulation as a function of time and (B) the same at the 190 hPa pressure level.
 195 Locations with 100 and 1000 times the specific humidity of the baseline simulation are indicated
 196 within the solid black contours. The vertical dashed line represents the end of the eruption.

197

198 As was the case with the initial global cooling following the eruption, the subsequent climate
 199 warming is regionally variable. The combination of the downwelling longwave from the increased
 200 stratospheric water vapor and the very cold and consolidated stratospheric winter polar vortex
 201 drives 15-30 K warm anomalies in January in northern North America and Siberia four years after
 202 the eruption ends (**Fig. 1, Fig. S8**). In July of simulation year 8, +10-20 K anomalies occurred on
 203 all continents with widespread +20-25 K in Antarctica. Nearly all continental areas on the planet
 204 have warmer than normal temperatures for years 5-13 of the simulation (1-9 years after the
 205 eruption ends). Continental areas with extreme heat (monthly mean temperatures $\geq 40^{\circ}\text{C}$) are
 206 dramatically expanded. In January of simulation year 8, such areas occur throughout the Amazon
 207 basin, south central South America, central and southern Africa, and much of central Australia.
 208 Monthly mean temperatures in some areas (the Amazon and east-central Australia) reach 49°C .
 209 July mean temperatures equal or exceed 40°C for the Sahara, the Arabian peninsula, and northwest
 210 portions of the Indian subcontinent, with extreme monthly mean temperatures $\geq 55^{\circ}\text{C}$ in southwest

211 Asia (**Fig. S8**). Even central North America has a small area with monthly mean temperatures of
212 40°C in July of simulation year 8.

213 Faster atmospheric circulation (limiting formation), removal of the tropical tropopause, and
214 subsequent moistening and cooling of the stratosphere produces massive ozone destruction. Our
215 simulations were conducted with a pre-industrial atmosphere, hence there is no anthropogenic
216 chlorine to catalyze ozone destruction. Global ozone loss averages 185 Dobson units (DU) during
217 simulation years 3-11, with middle and high latitude ozone loss exceeding 300 DU during winter
218 (**Fig. S9**).

219 Ocean circulation changes as well, with a general global slowing of near-surface current patterns.
220 The major currents of the northern hemisphere such as the Gulf Stream and Kuroshio are slowed
221 by 0.2-0.4 m/s, while the entire North Pacific gyre is displaced southward which weakens the north
222 equatorial current. The Antarctic Circumpolar current and the East Australian Current are least
223 impacted, but also see modest (~0.1 m/s) slowing. Reduced precipitation over continental areas
224 leads to reduced freshwater river discharge and salinification of the Arctic, North Atlantic, and
225 North and West-Equatorial Pacific oceans.

226 Despite these volatile changes to planetary climate during and following the eruption, conditions
227 return to or near pre-eruption by 11-16 years after the eruption ends. The H₂SO₄ aerosol is
228 removed even faster, and is completely gone from the atmosphere four years after the end of the
229 eruption (**Fig. S2**). Global surface temperatures return to within a few degrees of the baseline
230 simulation (**Fig. 1**), stratospheric water vapor mixing ratios return to ~3 ppm (**Fig. 3**), and the
231 ozone layer recovers (**Fig. S9**).

232 **4 Discussion and Conclusion**

233 With SO₂ emissions alone, our results support the CRB eruption as an agent that helped drive the
234 warm temperatures of the MMCO. Existing climate studies of the middle Miocene have had
235 trouble reconciling geological proxy evidence of warm global temperatures (~3°C above present)
236 with those of high, but not excessive CO₂ abundances (~350-400 ppm) (Tong et al., 2009; You et
237 al., 2009; Goldner et al., 2014; Henrot et al., 2010; Burls et al., 2021). Those studies have often
238 suggested changes in continental topography and albedo as well as ocean circulation differences
239 (associated with the open Central American and East Tethys Seaways (Henrot et al., 2010; Herold
240 et al., 2011)) as additional agents of climate warming. The literature suggests that up to 2°C of
241 warming is possible through the use of Miocene-appropriate surface and boundary conditions
242 alone (Burls et al., 2021). Our study did not aim to directly reproduce Miocene climate as we used
243 modern pre-industrial boundary conditions. Still, the warmth produced by SO₂ emissions from
244 the CRB eruptions, concentrated most strongly in the northern hemisphere continents and oceans,
245 could help to reconcile insufficiently low global CO₂ levels with regionally-variable climate
246 responses. Periodic eruptions of the CRB, which may have been phased over thousands or even
247 millions of years (Kasbohm and Schoene, 2018), would have helped generate this intermittent
248 warming response driven by stratospheric water vapor increases. Presumably (although further
249 simulations are needed to confirm), the addition of CO₂ emissions would only enhance this
250 warming and possibly help mitigate the initial cooling response seen in our eruption simulation.

251 Indeed, thermal maxima or hyperthermal events have occurred concurrently or near in time to
252 several flood basalt eruptions/large igneous province emplacements through Earth's history.
253 These include the Permian-Triassic, Paleocene-Eocene, and others and have been linked to major

254 eruptions such as the Siberian Traps and North Atlantic Igneous Province, respectively (Bond and
255 Sun, 2021; Gutjahr, 2017). As with the MMCO and CRB, a great deal of CO₂ is necessary to match
256 paleotemperature proxies from these events, and there remains a dispute if sufficient CO₂ was
257 emitted to explain these warm climates (Sobolev et al., 2011; Self et al., 2006; Armstrong McKay
258 et al., 2014). Black et al. (2018) modeled the Siberian Trap eruption climate impact and found
259 swings in climate between cooler sulfur-dominated periods and longer warm carbon-dominated
260 periods, however they did not include sulfur aerosol radiative heating which precluded the
261 tropopause warming that let water vapor flood into the stratosphere in our simulation. While our
262 results are consistent with sulfur emissions producing short-duration climate responses, we show
263 that sulfur alone can initiate climate warming, that is more intense and longer-lasting than the brief
264 cooling from shielding of shortwave radiation by sulfate aerosols, through the dynamical and
265 radiative response to stratospheric water vapor increases.

266 Our simulations thus challenge previous work that showed substantial decade-long climate cooling
267 from sulfur emissions (and hence sulfate aerosols) alone (Schmidt et al., 2016; Self et al. 2006).
268 The brief cooling we do see in the simulation within the first 1-3 years also does not increase land
269 or sea ice cover in a way that suggests sulfate aerosol cooling could initiate a positive feedback
270 with glaciation. North polar sea ice is above normal in area and does not exhibit seasonal melting
271 during the first 4 years of the simulation, but drops below normal for several years after the
272 eruption before then recovering. Similarly, widespread continental snow cover persists year-round
273 for much of northern Canada and Siberia during the eruption and immediately after, which would
274 tend to support glacial growth. However, the subsequent climate warming melts that snow cover
275 within ~3 years after the end of the eruption and eliminates that nascent development before it
276 could possibly reinforce the cooling through feedback processes.

277 These rapid climate variations would present challenges to the biosphere. The very high
278 continental summer temperatures would stress mammals with areas of >31°C wet bulb globe
279 temperatures expanded accordingly beyond baseline conditions. The likely fatal threshold of 35°C
280 wet bulb globe temperature for mammals is not exceeded anywhere on a monthly mean basis,
281 although transient periods with that level are possible (Sherwood et al., 2010). The increase and
282 then subsequent decrease in sea ice, coupled with a lack of seasonality could disrupt those
283 ecosystems dependent on sea ice. The ozone destruction would tend to increase surface ultraviolet
284 flux, but the presence of the H₂SO₄ aerosol layer, at least partially, ameliorates that threat. The
285 Siberian Traps eruption may have produced massive ozone destruction, primarily through the
286 concurrent emission of chlorinated species, which led to mutations among palynomorphs (Beerling
287 et al., 2007).

288 Mass extinctions and ocean anoxic events are closely correlated with flood basalt eruption/large
289 igneous province emplacement through the last 400 Ma of Earth's history. During the Miocene, a
290 comparatively modest extinction event occurred, often termed the "Middle Miocene disruption"
291 (Rapu et al., 1986). It followed the MMCO and was concurrent with the cooling of the MMCT.
292 Given our results, it seems more plausible that other factors following the CRB eruption (e.g., the
293 drawdown of CO₂ and the end of transient additional warming through the response to SO₂
294 emissions) were proximate to the extinction, rather than cooling driven by volcanic aerosols from
295 the CRB eruptions. However, most of the past extinctions associated with flood basalt eruptions
296 are believed to be due to associated climate warming (Reichow et al., 2009; Wignall, 2001;
297 Courtillot and Renne, 2003; Sobolev et al., 2011; Bond and Sun, 2021). Indeed, past mass

298 extinctions are correlated with $\geq 5.2^{\circ}\text{C}$ temperature increases, which our eruption simulation briefly
299 exceeds (Song et al., 2021).

300 The amount of water vapor in the stratosphere is a key metric for evaluating the evolution of any
301 terrestrial planet. Kasting et al. (1993) found a moist greenhouse limit of 3 parts-per-thousand
302 volume mixing ratio of H_2O vapor in the stratosphere based on diffusion-limited calculations of H
303 loss to space. Various three-dimensional climate models have found similar results with warm
304 ($>320\text{ K}$) surface temperatures (Wolf and Toon, 2015; Way et al., 2018; Popp et al., 2015) for a
305 rapidly-rotating planet like Earth, although that result is not uniform across all models (Leconte et
306 al., 2013). As the stratospheric water vapor mixing ratio in our eruption simulation exceeds this
307 threshold, our results point toward volcanically-induced transient moist greenhouse conditions
308 during major flood basalt eruptions. While planetary water loss through high altitude
309 photodissociation and escape may never have been a problem for Earth, that process is ongoing
310 for Mars and Venus. The role of volcanism in the evolution of climate and planetary water
311 inventory for both worlds is much debated (e.g., Solomon et al., 1999; Halevy and Head, 2014;
312 Kerber et al., 2015) and the possibility of exceeding the moist greenhouse limit during and
313 following major eruptions suggests possibly counteracting results. While a major eruption could
314 lead to periods of climate warmth for, e.g., early Mars, it may have also accelerated planetary water
315 loss by increasing the amount of water vapor at high altitudes that is more susceptible to
316 photodissociation and escape of hydrogen. Interestingly, (Bardeen et al., 2017) found similar
317 stratospheric moistening and ozone destruction while simulating the climate impacts of a major
318 asteroid impact and ejection of $\sim 15\text{ Tg}$ of soot into the atmosphere due to the subsequent global
319 fires, as well as a comparable $\sim 15\text{ year}$ duration to return to pre-event climate conditions.

320 Increases in stratospheric water vapor following volcanic eruptions has been measured after
321 Pinatubo and modeled for larger eruptions (Robock et al., 2009; Löffler et al., 2016; Joshi et al.,
322 2003). But the short duration of such eruptions prevents the removal of the tropical tropopause as
323 was seen in our simulation, and avoids a greater moistening of the stratosphere. Our results imply
324 that the long duration of flood basalt eruptions drives unique climate responses that do not occur
325 from classic stratovolcano eruptions such as Pinatubo, Toba, and Tambora. The long duration and
326 massive quantity of SO_2 emitted over years drives circulation responses that are ultimately more
327 impactful to the climate than the simple radiative response to the H_2SO_4 aerosols. Ultimately, the
328 difference in e-folding time in the removal of H_2SO_4 aerosols and that of the stratospheric water
329 vapor is a key metric. The sulfate aerosols are removed faster than water vapor from the
330 stratosphere, which allows the warming effect of the water vapor to dominate and persist longer
331 than the cooling provided by sulfate aerosol. Cooling from sulfate aerosols in our simulation
332 persists no longer than the eruption itself due to this fundamental difference in removal timescales.
333 This suggests that the “volcanic winter” (analogous to “impact winters” (Vellekoop et al., 2014))
334 paradigm of long-duration cold and darkness in response to massive flood basalt eruptions should
335 be reconsidered, and that any cooling is brief (although perhaps regionally intense) before a more
336 significant and long-duration warm response.

337 **Acknowledgments**

338 GEOSCCM is supported by the NASA MAP program and the high-performance computing
339 resources were provided by the NASA Center for Climate Simulation (NCCS).

340

341 **Open Research**

342 GEOSCCM model output is available on Zenodo at doi: 10.5281/zenodo.5420632.

343 **References**

Aquila, A., C. Baldwin, N. Mukherjee, E. Hackert, F. Li, J. Marshak, et al., Impacts of the eruption of Mount Pinatubo on surface temperatures and precipitation forecasts with the NASA GEOS subseasonal-to-seasonal system, *Journal of Geophysical Research: Atmospheres* **126**, e2021JD034830 (2021). doi: 10.1029/2021JD034830

Armstrong McKay, D.I., T. Tyrrell, P.A. Wilson, G.L. Foster, Estimating the impact of the cryptic degassing of Large Igneous Provinces: A mid-Miocene case-study, *Earth Planet. Sci. Lett.* **403**, 254–262 (2014).

Bardeen, C.G., R.R. Garcia, O.B. Toon, A.J. Conley, On Transient Climate Change at the Cretaceous-Paleogene Boundary due to Atmospheric Soot Injections, *Proceedings of the National Academy of Sciences of the United States of America* **114**, 36, E7415-7424 (2017). doi:10.1073/pnas.1708980114

Barry, T.L., S. Self, S.P. Kelley, S. Reidel, P. Hooper, and M. Widdowson, New ⁴⁰Ar/³⁹Ar dating of the Grande Ronde lavas, Columbia River Basalts, USA: Implications for duration of flood basalt eruption episodes, *Lithos* **118**, 3-4, 213-222 (2010). <https://doi.org/10.1016/j.lithos.2010.03.014>.

Beerling, D.J., M. Harfoot, B. Lomax, J.A. Pyle, The stability of the stratospheric ozone layer during the end-Permian eruption of the Siberian Traps, *Phil. Trans. R. Soc. A.* **365**, 1843–1866 (2007), <http://doi.org/10.1098/rsta.2007.2046>

Black, B.A., R.R. Neely, JF Lamarque, *et al.*, Systemic swings in end-Permian climate from Siberian Traps carbon and sulfur outgassing, *Nature Geosci* **11**, 949–954 (2018). <https://doi.org/10.1038/s41561-018-0261-y>

Bluth, G.J.S., S.D. Doiron, C.C. Schnetzler, A.J. Krueger, L.S. Walter, Global Tracking of the SO₂ Clouds from the June, 1991 Mount Pinatubo Eruptions, *Geophysical Research Letters* **19**(2), 151-154 (1992). doi: 10.1029/91GL02792.

Burls, N.J., C.D. Bradshaw, A.M. De Boer, N. Herold, M. Huber et al., Simulating Miocene warmth: Insights from an opportunistic multi-model ensemble (MioMIP1). *Paleoceanography and Paleoclimatology* **36**, e2020PA004054 (2021). <https://doi.org/10.1029/2020PA004054>

Colarco, P., A. Da Silva, M. Chin, T. Diehl, Online simulations of global aerosol distributions in the NASA GEOS-4 model and comparisons to satellite and ground-based aerosol optical depth, *J. Geophys. Res.* **115**(D14), D14207 (2010). doi:10.1029/2009JD012820.

Courtillot, V.E., P. R. Renne, On the ages of flood basalt events, *C. R. Geosci.* **335**, 113–140 (2003).

Davis, K.N., J. A. Wolff, M. C. Rowe, O. K. Neill, Sulfur release from main-phase Columbia River Basalt eruptions, *Geology* **45** (11), 1043–1046 (2017). doi: <https://doi.org/10.1130/G39371.1>

Duncan, B.N., S.E. Strahan, Y. Yoshida, S.D. Steenrod, N. Livesey, Model study of cross-tropopause transport of biomass burning pollution, *Atmos. Chem. Phys.*, **7**, 3713-3736 (2007).

Foster, G.L., C.H. Lear, J.W.B. Rae, The evolution of pCO₂, ice volume and climate during the middle Miocene, *Earth Planet. Sci. Lett* **341–344**, 243–254 (2012).

- Glaze, L.S., S. Self, A. Schmidt, S.J. Hunter, Assessing Eruption Column Height in Ancient Flood Basalt Eruptions, *Earth and Planetary Science Letters* **457**, 263-270 (2017). doi: 10.1016/j.epsl.2014.07.043.
- Goldner, A., N. Herold, M. Huber, The Challenge of Simulating the Warmth of the mid-Miocene Climatic Optimum in CESM1, *Climate of the Past* **10**, 523-536 (2014). doi: 10.5194/cp-10-523-2014
- Griffies, S.M., A. Gnanadesikan, K.W. Dixon, J.P. Dunne, R. Gerdes, M.J. Harrison, et al., Formulation of an ocean model for global climate simulations, *Ocean Science* **1**, 45-79 (2005).
- Griffies, S.M., R. J. Greatbatch, Physical processes that impact the evolution of global mean sea level in ocean climate models, *Ocean Modelling* **51**, 37-72 (2012). doi:10.1016/j.ocemod.2012.04.003.
- Gutjahr, M., A. Ridgwell, P. Sexton, et al., Very large release of mostly volcanic carbon during the Palaeocene–Eocene Thermal Maximum, *Nature* **548**, 573–577 (2017).
<https://doi.org/10.1038/nature23646>
- Halevy, I., J. Head III, Episodic warming of early Mars by punctuated volcanism. *Nature Geosci* **7**, 865–868 (2014). doi:10.1038/ngeo2293
- Head III, J.W., et al., Flood Volcanism in the Northern High Latitudes of Mercury Revealed by MESSENGER, *Science* **333** (6051), 1853-1856 (2011). doi: 10.1126/science.1211997.
- Henrot, A.-J., L. François, E. Favre, M. Butzin, M. Ouberdous, G. Munhoven, Effects of CO₂, continental distribution, topography and vegetation changes on the climate at the Middle Miocene: a model study, *Clim. Past* **6**, 675–694 (2010). <https://doi.org/10.5194/cp-6-675-2010>
- Herold, N., M. Huber, R.D. Müller, Modeling the Miocene Climatic Optimum. Part I: Land and Atmosphere, *Journal of Climate* **24**(24), 6353-6372 (2011). doi: 10.1175/2011JCLI4035.1
- Hodell, D.A., F. Wodruff, Variations in the strontium isotopic ratio of seawater during the Miocene: stratigraphic and geochemical implications, *Paleoceanography* **9**, 405-426 (1994).
- Hunke, E.C., W. H. Lipscomb, “CICE: The Los Alamos Sea Ice Model, Documentation and Software Manual, Version 4.0” (Technical Report, Los Alamos National Laboratory, 2008).
- Jacobson, M.Z., Computation of global photochemistry with SMVGear II, *Atmos. Environ.* **29**, 2541–2546 (1995).
- Jaeger, W.L. et al., Emplacement of the youngest flood lava on Mars: A short, turbulent story, *Icarus* **205**(1), 230-243 (2010). <https://doi.org/10.1016/j.icarus.2009.09.011>.
- Jerram, D.A., M. Widdowson, The anatomy of Continental Flood Basalt Provinces: geological constraints on the processes and products of flood volcanism, *Lithos* **79**, 3-4 385-405 (2005).
<https://doi.org/10.1016/j.lithos.2004.09.009>.
- Joshi, M.M., K.P. Shine, A GCM Study of Volcanic Eruptions as a Cause of Increased Stratospheric Water Vapor, *Journal of Climate* **16**(21), 3525-3534 (2003). doi: 10.1175/1520-0442(2003)016<3525:AGSOVE>2.0.CO;2
- Kasbohm, J., B. Schoene, Rapid eruption of the Columbia River flood basalt and correlation with the mid-Miocene climate optimum, *Science Advances* **4**(9), eaat8223 (2018). doi: 10.1126/sciadv.aat8223
- Kasting, J.F., D.P. Whitmire, R.T. Reynolds, Habitable Zones Around Main Sequence Stars, *Icarus* **101**, 1, 108-128 (1993). doi: 10.1006/icar.1993.1010

- Kerber, L., F. Forget, R. Wordsworth, Sulfur in the Early Martian Atmosphere Revisited: Experiments with a 3-D Global Climate Model, *Icarus* **261**, 133-148 (2015). doi:10.1016/j.icarus.2015.08.011
- Kirchner, I., G.L. Stenchikov, H.-F. Graf, A. Robock, A., J.C. Antuña, Climate model simulation of winter warming and summer cooling following the 1991 Mount Pinatubo volcanic eruption, *J. Geophys. Res.* **104**(D16), 19039–19055 (1999). doi:10.1029/1999JD900213.
- Kürschner, W.M., Z. Kvacek, D.L. Dilcher, The impact of Miocene atmospheric carbon dioxide fluctuations on climate and the evolution of terrestrial ecosystems, *Proc. Natl. Acad. Sci.* **105**, 440-453 (2008).
- Lancaster, M.G., et al., Great Lava Flow Fields on Venus, *Icarus* **118**(1), 69-86 (1995). <https://doi.org/10.1006/icar.1995.1178>.
- Leconte, J., F. Forget, B. Charnay *et al.*, Increased insolation threshold for runaway greenhouse processes on Earth-like planets, *Nature* **504**, 268–271 (2013). doi: 10.1038/nature12827
- Löffler, M., S. Brinkop, P. Jöckel, Impact of major volcanic eruptions on stratospheric water vapour, *Atmos. Chem. Phys.* **16**, 6547–6562 (2016). doi:10.5194/acp-16-6547-2016
- Nielsen, J.E., S. Pawson, A. Molod, B. Auer, A. M da Silva, A. R. Douglass, B. Duncan, Q. Liang, M. Manyin, L. D. Oman, W. Putman, S. E. Strahan, K. Wargan, Chemical mechanisms and their applications in the Goddard Earth Observing System (GEOS) earth system model, *J. Adv. Model. Earth Syst.* **9**, 3019–3044 (2017). doi:10.1002/2017MS001011
- O'Hara, M.J., Flood Basalts and Lunar Petrogenesis, *Journal of Petrology* **41**(7), 1121-1125 (2000)..
- Popp, M.,H. Schmidt, J. Marotzke, Transition to a Moist Greenhouse with CO₂ and solar forcing, *Nat Commun* **7**, 10627 (2016). doi:10.1038/ncomms10627
- Rampino, M.R., R.B. Stothers, Flood Basalt Volcanism During the Past 250 Million Years, *Science* **241**, 4866, 663-668 (1998). doi:10.1126/science.241.4866.663.
- Raup, D.M., J.J. Sepkoski Jr., Periodic Extinction of Families and Genera, *Science* **231**, 4740, 833-836 (1986). doi: 10.1126/science.11542060.
- Reichow, M.K., A.D. Saunders, M.S. Pringle, A.I. Al'Mukhamedov, A.Y. Medvedev, M.B. Allen, V.L. Andreichev, M.M. Buslov, G.S. Fedoseev, I.Y. Safonova, C.E. Davies, J.G. Fitton, S. Inger, C. Mitchell, V.N. Puchkov, R.A. Scott, The timing and extent of the eruption of the Siberian Traps large igneous province: Implications for the end-Permian environmental crisis, *Earth Planet. Sci. Lett.* **277** (1–2), 9-20 (2009).
- Reidel, S.P., The Columbia River Basalt Group: A flood basalt province in the Pacific Northwest, USA, *Geosci. Can.* **42**, 151–168 (2015).
- Rienecker, M.M., et al., "The GEOS-5 data assimilation system — Documentation of versions 5.0.1, 5.1.0, and 5.2.0" (NASA Tech. Memo., NASA TM-2008-104606, vol. 27, 118 pp, 2008)
- Robock, A., Volcanic eruptions and climate, *Reviews of Geophysics* **38**, 191–219 (2000).
- Robock, A., C.M. Ammann, L. Oman, D. Shindell, S. Levis, and G. Stenchikov, Did the Toba volcanic eruption of ~74k BP produce widespread glaciation? *J. Geophys. Res.* **114**, D10107 (2009). doi:10.1029/2008JD011652.
- Schmidt, A., R.A. Skeffington, T. Thordarson, S. Self, P.M. Forster, A. Rap, et al., Selective environmental stress from sulphur emitted by continental flood basalt eruptions, *Nature Geoscience* **9**(1), 77–82 (2016).

Self, S., T.Thordarson, M. Widdowson, Gas Fluxes from Flood Basalt Eruptions, *Elements* **1** (5), 283–287 (2005). doi: <https://doi.org/10.2113/gselements.1.5.283>.

Self, S., M. Widdowson, T. Thordarson, A.E. Jay, Volatile fluxes during flood basalt eruptions and potential effects on the global environment: A Deccan perspective, *Earth and Planetary Science Letters* **248**(1-2), 518-532 (2006).

Sherwood, S.C., M. Huber, An adaptability limit to climate change due to heat stress, *Proceedings of the National Academy of Sciences* **107** (21), 9552-9555 (2010). doi:10.1073/pnas.0913352107
Sobolev, S., Sobolev, A., Kuzmin, D. *et al.*, Linking mantle plumes, large igneous provinces and environmental catastrophes, *Nature* **477**, 312–316 (2011). <https://doi.org/10.1038/nature10385>

Solomon, S.C., M.A. Bullock, D.H. Grinspoon, Climate Change as a Regulator of Tectonics on Venus, *Science* **286**, 5437, 87-90 (1999). DOI: 10.1126/science.286.5437.87

Song, H., D.B. Kemp, L. Tian, L. *et al.*, Thresholds of temperature change for mass extinctions, *Nat Commun* **12**, 4694 (2021). doi:10.1038/s41467-021-25019-2

Sosdian, S.M., T.L. Babila, R. Greenop, *et al.*, Ocean Carbon Storage across the middle Miocene: a new interpretation for the Monterey Event, *Nat Commun* **11**, 134 (2020). <https://doi.org/10.1038/s41467-019-13792-0>

Stoffel, M., M. Khodri, C. Corona *et al.*, Estimates of volcanic-induced cooling in the Northern Hemisphere over the past 1,500 years, *Nature Geosci* **8**, 784–788 (2015). <https://doi.org/10.1038/ngeo2526>

Strahan, S.E., B.N. Duncan, P. Hoor, Observationally derived transport diagnostics for the lowermost stratosphere and their application to the GMI chemistry and transport model, *Atmos. Chem. Phys.* **7**, 2435–2445 (2007). doi: 10.5194/acp-7-2435-2007

Tong, J.A., Y. You, R.D. Müller, M. Seton, Climate model sensitivity to atmospheric CO₂ concentrations for the middle Miocene, *Global Planet. Change* **67**, 129–140 (2009).

Vellekoop, J., A.Sluijs, J. Smit, S. Schouten, J. W. H.Weijers, J. S. Sinninghe Damsté, H. Brinkhuis, Rapid short-term cooling at K–Pg boundary, *Proceedings of the National Academy of Sciences* **111** (21), 7537-7541 (2014). DOI:10.1073/pnas.1319253111

Way, M.J., A.D. Del Genio, I. Aleinov *et al.*, Climates of Warm Earth-like Planets I. 3D Model Simulations, *The Astrophysical Journal Supplemental Series* **239**, 24 (2018). doi: 10.3847/1538-4365/aae9e1

Wignall, P.B., Large igneous provinces and mass extinctions, *Earth Sci. Rev.* **53**, 1–33 (2001).

Wolf, E.T., OB. Toon, The evolution of habitable climates under the brightening Sun. *J. Geophys. Res. Atmos.* **120**, 5775– 5794 (2015). doi: 10.1002/2015JD023302.

You, Y., M. Huber, R.D. Müller, C.J. Poulsen, J. Ribbe, Simulation of the Middle Miocene Climate Optimum, *Geophys. Res. Lett.* **36**, L04702 (2009). doi:10.1029/2008GL036571

Zambri, B., A.N. LeGrande, A. Robock, J. Slawinska, Northern Hemisphere winter warming and summer monsoon reduction after volcanic eruptions over the last millennium, *J. Geophys. Res. Atmos.* **122**, 7971– 7989 (2017). doi:10.1002/2017JD026728